Virus removal and inactivation in a hybrid microfiltration-UV process with a photocatalytic membrane

Accepted for publication in the *Separation and Purification Technology* journal

on May 28, 2015.

Published article DOI: 10.1016/j.seppur.2015.05.039

Bin Guo, Elodie L. Pasco, Irene Xagoraraki, Volodymyr V. Tarabara*

Department of Civil and Environmental Engineering, Michigan State University,

East Lansing, MI 48824, USA

Emails:

guobin@msu.edu (BG)

elodiepasco@gmail.com (EP)

xagorara@egr.msu.edu (IX)

tarabara@msu.edu (VT)

*Corresponding author: Phone: +1 (517) 432-1755; Email: tarabara@msu.edu

Keywords:

UV disinfection, microfiltration, titanium dioxide, photocatalytic membrane reactor, virus

Abstract

The study describes the first application of photocatalytic membranes for virus removal and inactivation. In the proposed hybrid treatment process, a UV lamp and a microfiltration membrane are positioned in foci of two parabolic reflectors facing each other and UV light is focused on a photocatalyst-coated outer surface of the microfilter. The ceramic tubular membrane (nominal pore size of 0.8 μm) is operated in an inside-out geometry. To evaluate virus removal and inactivation efficiency of the hybrid photocatalytic UV-MF process, bacteriophage P22 is used as a model virus. The kinetics of P22 inactivation by direct UV is found to fit Collins-Selleck model with the coefficient of specific lethality Λ_{CS} = 1.972. Batch UV disinfection and crossflow filtration tests with membranes coated or uncoated with a layer of photocatalyst show that the hybrid photocatalytic UV-microfiltration process is considerably more effective in inactivating the virus (LRV = 5.0 ± 0.7) than the constituent processes - UV disinfection and microfiltration - applied in series (aggregate LRV = 2.0 ± 0.5) or together but without the photocatalytic coating on the membrane (LRV = 2.4 ± 0.2). Potential applications of the proposed treatment process include disinfection of turbid, high fouling potential and high flow rate streams.

1. Introduction

Photocatalytic membrane reactors (PMRs) combine membrane separation and photocatalysis in one hybrid process [1, 2]. PMR is a highly versatile technology due to the range of engineering designs it affords and the realm of possible applications. Water treatment is a salient example of such application area. Since 1985 when Matsunaga et al. [3] used Pt-loaded TiO_2 for catalytic inactivation of three types of bacteria, applications of photocatalysis to water disinfection have been growing [4]. Indeed, there is a large body of literature on the use of photocatalysis for inactivating microorganisms in water [5, 6]. Notably, photocatalytic treatment can be highly effective with respect to viruses (e.g. [7-10]). Most of the PMR-based water treatment work, however, has focused on chemical pollutants. To our knowledge, there have been only five reports on the application of photocatalytic membranes to water disinfection [11-15]. All five studies were on *E. Coli* control and three of the five [13-15] also used silver, a known bactericide, as a component of photocatalytic membranes. Several studies (e.g. [16]) also explored how an added photocatalytic function can help improve membrane's resistance to biofouling.

Various PMRs have been implemented that employ different types of light sources and membranes. UV lamps have been the most common choice of the source of photons although new visible light catalyst materials make using visible light possible [17]. Because of the ability to support oxidation reaction, ceramic membranes have been used much more commonly than their polymeric and nanocomposite counterparts [18]. Many different photocatalytic materials have been explored as well, with TiO_2 being by far the most studied and applied photocatalyst [17, 19].

PMRs can be categorized into two major groups: a) PMRs with the catalyst materials suspended in the bulk of the feed solution and b) reactors where the catalyst is immobilized on the membrane surface. In the latter case, typically it is the feed surface of the membrane that supports the catalyst. By illuminating such surface with UV light, photocatalysis occurs in the immediate vicinity of the separation layer bringing about

potential additional advantages of fouling control and retentate disinfection. This PMR configuration, however, couples separation and catalytic properties of the membrane making their optimization more challenging. An alternative configuration is when it is the membrane support layer (i.e. permeate side of the membrane) that is photocatalytic. To our knowledge, the only study that explored such configuration is the work by Bosc et al. [20]. One major benefits of such approach is the possibility of an independent control of the separation and photocatalytic functions. Another benefit is an extension of the first: by regulating what materials are retained by the membrane, one can control the make-up of the permeate solution to improve the photocatalytic function. For example, catalyst poisons or particulates capable of shielding UV light may be removed at the feed-membrane interface to make photocatalysis on the permeate side more efficient. The choice of PMRs configuration has implications for the design of the catalytic layer. Because most practicable membranes are asymmetric, the feed and permeate faces of membranes have dramatically different morphologies. The membrane “skin” (i.e. the feed side) has much smaller pores and, typically, a much smoother surface than the permeate side. This implies that different coating strategies might be needed to form photocatalytic layers on these supports.

The goal of this work is to extend the PMR design concept proposed by Bosc et al. [20] to tubular membranes and to apply such PMR to photocatalytic disinfection of viruses. We employ P22 bacteriophage as a model virus and compare the performance of the proposed PMR against that of its constituent processes – UV disinfection and microfiltration. To our knowledge, this is the first application of photocatalytic membranes to virus removal or inactivation.

2. Experimental

2.1. Reagents

Aeroxide TiO_2 P25 powder was provided by Evonik Industries. Lysozyme (from chicken egg white), ethylenediaminetetraacetic acid (EDTA) and phosphoric acid were purchased from Sigma-Aldrich. Trypticase soy broth (TSB), trypticase soy agar (TSA) and Bacto agar were purchased from Becton, Dickinson and Co. Glycerol and sodium hydroxide were obtained from Avantor Performance Materials. KI/KIO_3 solution was a mixture of 0.6 M potassium iodide (Jade Scientific) and 0.1 M iodate (EM Industries) in 0.01 M borate buffer (Sigma-Aldrich). Ultrapure water (~ 17 MΩ/cm) was produced by a Barnstead E-pure water purification system (Thermo Fisher Scientific). The bacteriophage was propagated by inoculating 25 mL trypticase soy broth with Salmonella enterica serovar Typhimurium LT2 and allowing for growth at 37°C.

2.2. Bacteriophage propagation and preparation of feed suspension

To evaluate virus removal and inactivation efficiency of the hybrid photocatalytic UV-MF process, bacteriophage P22 was used as a model virus. P22 is a dsDNA virus [21-25] that has been used as a surrogate for human viruses to study their attenuation [25] and their fate in sewage [26]. The bacteriophage was propagated by inoculating 25 mL trypticase soy broth with Salmonella enterica serovar Typhimurium LT2 and allowing for growth at 37 °C. After overnight incubation, 0.1 mL of lysozyme (50 mg/mL) and 0.75 mL of 0.5 M EDTA were added to lyse host bacterial cells. The culture was then centrifuged at 4000 rpm for 10 min and the supernatant was filtered through a 0.45 µm sterile syringe filter unit (EMD Millipore). The resulting P22 stock suspension had P22 concentration of $5 \cdot 10^9$ PFU/mL and was maintained at 4 °C. The P22 bacteriophage feed suspension used in all disinfection and filtration experiments was prepared by diluting 300 µL of P22 stock in 3 L of ultrapure water and thus had P22 concentration of ~ $5 \cdot 10^5$ PFU/mL.

2.3. Membranes and deposition of photocatalytic coating on their surface

Membranes used in all tests were TiO_2 tubular ceramic microfilters (TAMI Industries) with a nominal pore size of 0.8 μm, 25 cm in length, outer diameter of 1 cm and the inner diameter of 0.6 cm. The permeate side of the membrane was coated with commercial Aeroxide TiO_2 P25 powder (50 ± 15 m^2/g, 78-85% anatase and 14-17% rutile [27], mean particle size of 21 nm) by dip-coating the membrane with a 10 wt% TiO_2 solution prepared following the procedure described by Wang et al. [28]. Prior to its use in the dip-coating procedure, the TiO_2 suspension was stirred and sonicated for 24 h. The tubular ceramic membrane with both ends sealed by Parafilm (to avoid coating the internals walls of the membrane channel) was vertically dipped into the TiO_2 suspension, maintained submerged for 30 s, and then withdrawn at a constant speed of 4.7 cm/min. The dip-coating instrument was constructed in-house using a syringe pump (55-2219, Harvard apparatus). The entire procedure included 10 coating cycles with 5 min drying at 80°C after the deposition of each coat. After the tenth coating cycle, the membrane was dried at 80°C for 24 h, and then calcined in a furnace (RHF 15/3, Carbolite Ltd). The furnace temperature was programmed to increase to 500 °C with a ramp rate of 4.0 °C/min, stay constant for 45 min, and finally decrease to the room temperature at a rate of 4.0 °C/min.

2.4. Membrane cleaning

Prior to each filtration experiment, the membrane was cleaned by following the procedure recommended by the membrane supplier: the membrane was first soaked in 20 g/L NaOH at 85 °C for 30 min, rinsed with ultrapure water to bring pH to 7, soaked in 75% H_3PO_4 at 50 °C for 15 min, and then again rinsed with DI water to bring pH to 7. The efficacy of cleaning was verified by performing a pure water flux test and comparing membrane resistances before and after cleaning.

2.5. Hybrid UV-membrane filtration unit: Design and operation

Figure 1 shows the schematic of the hybrid MF-UV disinfection unit used in all filtration experiments. The membrane and the UV lamp were placed in the foci of two alumina parabolic reflectors (Fig. 2) positioned to face each other at a distance that could be adjusted to regulate UV fluence on the membrane surface. The parabolic design ensured that the outer surface of the membrane was evenly irradiated by the UV light. UV-C irradiation was generated by a preheated germicidal UV lamp (16 W, model GPH330T5L/4, Atlantic Ultraviolet Corp.) The crossflow was provided by a peristaltic pump (model 621 CC, Watson-Marlow) equipped with a pulsation dampener (AD-10 PS, Yamada America). Transmembrane pressure was measured by pressure gauges (0 to 15 psi range, Ashcroft) installed on the feed and retentate sides of the membrane unit. The crossflow flux was measured using a flowmeter (model 101-8, McMillan). Permeate was collected on an electronic mass balance (Adventurer Pro AV8101C, Ohaus) interfaced with a data acquisition system (model NI PCI-6221, National Instruments).

All filtration tests were performed in a constant pressure mode with the average transmembrane pressure of 2.8 ± 0.2 psi (19.4 ± 1.5 psi). Average pressure values in filtration tests of different types were 2.67 ± 0.14 psi, 2.83 ± 0.14 psi, and 2.95 ± 0.30 psi in experiments on MF only, UV +MF with non-catalytic membranes, and UV + MF photocatalytic membrane, correspondingly (see Supplementary Content (SC), Table S1). The membrane, which was operated in an inside-out flow geometry, was housed in a quartz sleeve (160 mm in length, 20.5 mm in outer diameter) to allow for both illumination of the permeate side of the membrane by UV light and permeate collection. At the membrane ends, the space between the membrane and the quartz sleeve was sealed using two silicone stoppers (Fig. 2). The permeate was allowed to leave the quartz sleeve through a syringe needle into the permeate collection tube and the permeate mass flow rate was recorded at 1 s intervals. The average crossflow rate was 1.06 ± 0.09 L/min translating into the average crossflow velocity of 0.62 ± 0.05 m/s.

Average crossflow rate values in filtration tests of different types were 1.1 ± 0.0 L/min, 1.0 ± 0.1 L/min, and 1.1 ± 0.0 L/min in experiments on MF only, UV +MF with non-catalytic membranes, and UV + MF photocatalytic membrane, correspondingly (see SC, Table S1).

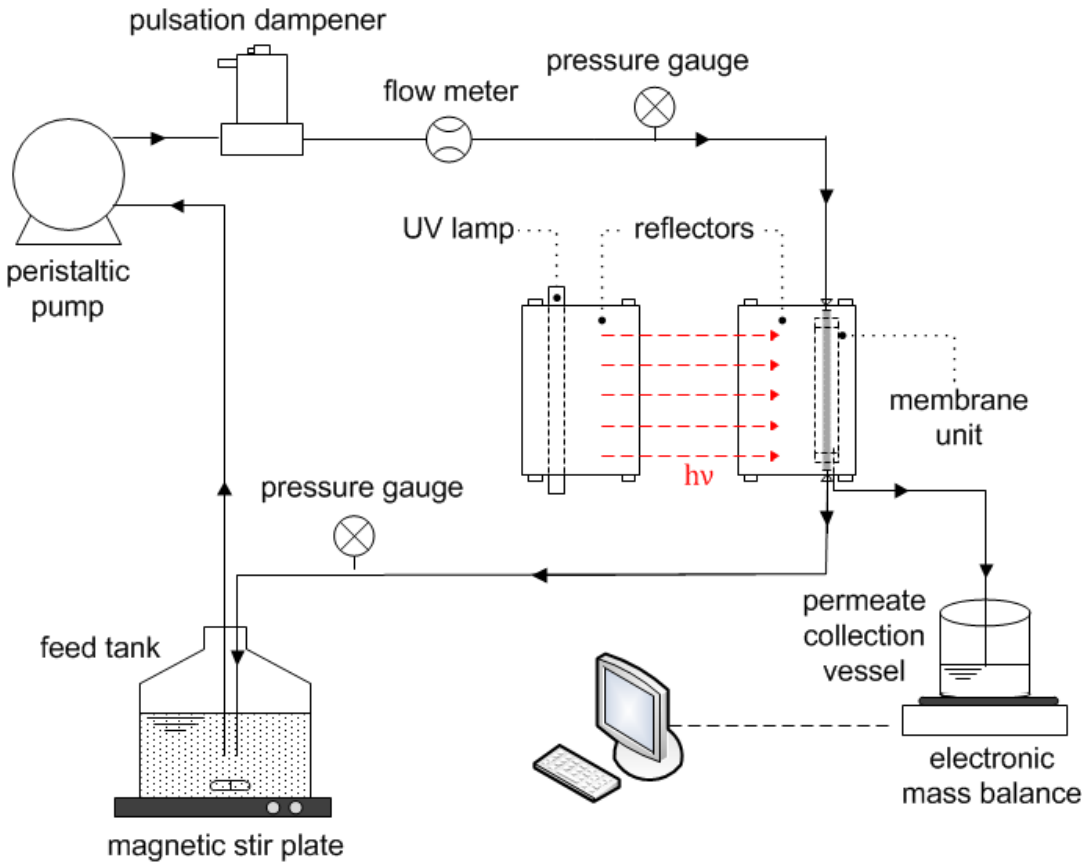

Figure 1. Schematic diagram of the hybrid membrane filtration-UV treatment system.

Temperature of the permeate as a function of filtration time and UV exposure was measured in real time in a separate crossflow test with the membrane tilted at an angle to fasten permeate collection and minimize heat loss prior to the measurement. The samples of permeate were collected in a 2 mL vial (2 mL) periodically for 2 h. The temperature of the solution was measured with a digital thermometer (model S407993; Fisher Scientific: accuracy: ±1°C).

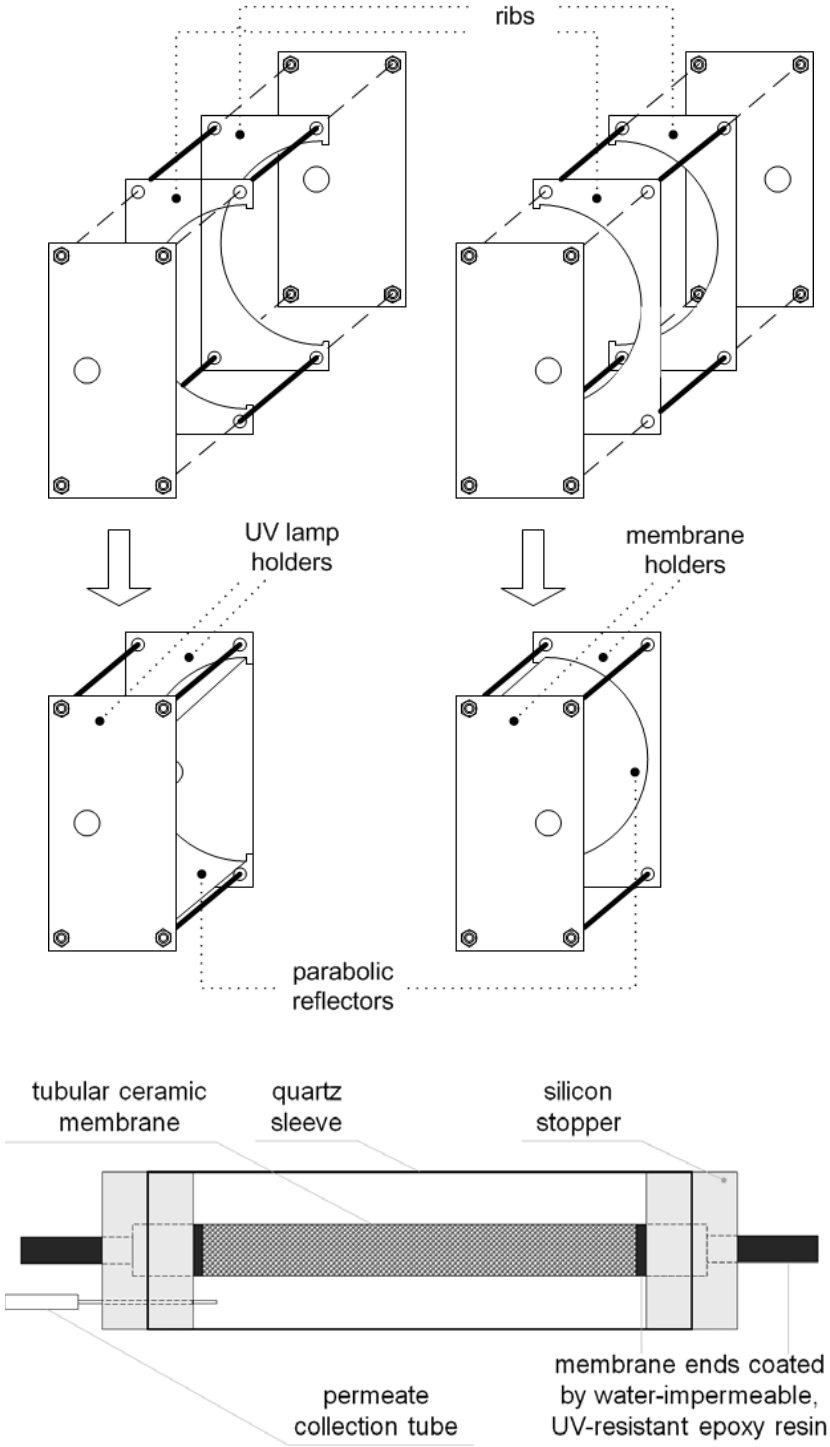

Figure 2. Design of custom-made parabolic UV light reflectors and the membrane housing unit. The membrane housing unit is drawn not to scale. Membrane's length and outer diameter are 0.25 m and 0.01 m, respectively.

2.6 Sample collection and storage

Samples of the feed solution were withdrawn from the feed tank before and after each filtration experiment. In each filtration test, permeate samples were collected immediately after the start of filtration as well as 10, 20, 30, 45 and 60 min into the experiment. Each sample was divided into two aliquots. One aliquot was placed in a glass vial with a plastic cap, wrapped in foil, and stored at 4 °C. The second aliquot was frozen in a 5mL cryogenic vial at -80°C as a backup. The cryoprotectant (20% glycerol) to sample volume ratio was 1:1.

2.7. UV dose quantification

Chemical actinometry [29-31] was used to measure UV fluence by determining the UV absorbance of KI/KIO_3 solution. The exposure of the KI/KIO_3 solution to UV light results in the formation of triiodide, the concentration of which can be determined spectrophotometrically at 352 nm (MultiSpec 1501, Shimadzu). For each measurement, the absorbance of the KI/KIO_3 solution in dark was used as a baseline. To determine the quantum yield Φ (mole of product formed per mole of photons absorbed), the concentration of KI was first measured by recording KI absorbance at 300 nm and applying the Beer-Lambert law: $C_{KI} = \frac{1}{\ell}\frac{A_{300}}{\varepsilon_{300}}$, where A_{300} and ε_{300} =1.061 M^{-1} cm^{-1} are the absorbance of KI at 300 nm and the extinction coefficient of KI at 300 nm, respectively [32], and ℓ = 1 cm is the optical path length of the spectrophotometer cell. With C_{KI} known, Φ was computed as:
$\Phi = 0.75(1 + (T - 20.7))(1 + (C_{KI} - 0.577))$, where T is the solution temperature in ^{o}C.

Fluence F (mJ/cm^2) is given by [32]

$$F = \frac{n}{\Phi}\frac{\Delta A_{352}}{\varepsilon_{352}\ell}\frac{V_s}{S_s} \quad (1)$$

where n = 4.72·10^5 (J·E^{-1}) is a conversion factor for 254 nm wavelength, ε_{352} = 27,600 $M^{-1}cm^{-1}$ is the extinction coefficient of triiodide at 352 nm [33], V_s (mL) is the total volume

of solution in the quartz sleeve, and S_s = 96.6 cm^2 is the surface area of the quartz sleeve exposed to UV light.

2.8. Quantifying the efficacy of disinfection by direct UV only

The disinfection efficacy of UV light in the crossflow system in the absence of photocatalyst could not be measured because the possibility of a photocatalytic effect could not be eliminated. Instead, to quantify virus inactivation due to UV only we employed the following multistep procedure:

Step 1: Measuring the permeate retention time in the quartz sleeve. Based on the measured values of the permeate mass flow rate, $\dot{m}_p$, and the mass of the residual permeate solution, m_r, in the quartz sleeve, the retention time of permeate solution was calculated as $\mathrm{t} = \frac{\mathrm{L}}{\mathrm{v}}$, where L is the length of the quartz sleeve (L = 15 cm); $v = \frac{\dot{m}_p}{\rho \cdot A_r}$ is the flux of permeate solution in quartz sleeve, ρ is the density of permeate solution and $A_r = \frac{m_r}{\rho \cdot L}$ is the cross-sectional area of the residual permeate solution in the sleeve.

Step 2: Relating UV fluence to permeate retention time. This was done by placing the KI/KIO_3 indicator solution in the permeate chamber (the quartz sleeve) of the hybrid UV-MF unit, without applying any pressure or crossflow and exposing the solution to UV. Because the permeate retention time values calculated at Step 1 did not exceed 30 s in any of the experiments, the KI/KIO_3 solution was exposed to UV irradiation for 5, 10, 20 and 30 s. Based on these measurements, the dependence of UV fluence on retention time was established.

Step 3: Determining P22 inactivation as a function of UV fluence. To determine the dependence of P22 inactivation efficiency on UV fluence, P22 suspensions were exposed to UV for 5, 10, 15, 20 and 30 s in a sequence of separate tests. The obtained values of P22 inactivation (see section 2.10) were related to UV fluence using the relationship established at step 2.

Following the above three steps, the P22 removal efficacy was related to the mass flow rate. Thus, in each test of the hybrid microfiltration-UV process, the contribution of direct UV to virus inactivation could be determined.

2.9. Electron microscopy of the membrane surface

Scanning electron microscopy (SEM) images of the tubular membrane surface as well as the membrane's cross-section were recorded (JEOL 6610LV SEM) under magnifications of ×700 and ×1000. Membrane samples for SEM imaging were obtained by breaking the membrane, mounting a piece with membrane's cross-section exposed onto an aluminum stub and coating the mounted sample with ~ 20 nm thick layer of gold (Emscope Sputter Coater, model SC 500, Quorum Technologies).

2.10. Quantification of the viable bacteriophage

The concentration of viable P22 bacteriophage was quantified by plaque assaying. TSA plates (1.5%) and 1% top agar tubes were prepared according to the standard method [34]. On the same day as the experiment, the *Salmonella enterica serovar Typhimurium LT2* stock was removed from -80 ºC and defrosted. One milliliter of the defrosted stock was introduced into 10 mL TSB media under sterile conditions and placed in a 37 °C incubator. After overnight incubation, 1 mL *Salmonella enterica serovar Typhimurium LT2* culture was transferred to 30 mL TSB at 37 °C for 3 h to reach the log phase of growth. The concentrations of viable P22 in feed solution and filtrate samples were determined by the double agar layer method [34]. First, top agar tubes were boiled and then placed in a 45-48 °C water bath. A series of dilutions (10^1 to 10^4) was prepared for each sample and each diluted sample was analyzed in triplicate. Second, one top agar tube was removed from the water bath, 0.3 mL of log phase *Salmonella enterica serovar Typhimurium LT2* culture and 1 mL of sample were sequentially added. Then, the mixture was gently agitated and poured on a 1.5% TSA bottom agar plate. Slight shaking and swirling was applied to distribute the agar evenly on the plate. After the top agar hardened at room temperature, the plates were inverted and incubated for 16 to 18 h at 37 °C. Finally, the number of circular clear spots in each

lawn of host bacteria was counted to determine plaque-forming units (PFU/mL) for each sample.

2.11. Quantification of the total bacteriophage

The total P22 bacteriophage count, which includes both the viable (infective) and non-viable (non-infective) virus, was determined by qPCR. Within 24 h of the filtration experiment, DNA of the bacteriophage was extracted using a MagNA Pure automatic extraction machine and MagNA Pure Compact Nucleic Acid Isolation Kit (Roche Diagnostics Corp). Samples (390 µL each) were extracted with 10 µL carrier RNA (1 µg/µL, Qiagen) to obtain 100 µL eluates. Carrier RNA was added to prevent DNA adsorption on the surfaces of the extraction kit. The nucleic acid eluents were stored at −20 °C. Each eluate was analyzed by real-time qPCR in triplicate following the procedure described by Masago et al. [25] (also see SC; Table S2). Each sample that was subjected to qPCR analysis consisted of 5 µL nucleic acid eluates, 10 µl of qPCR master mix (LightCycler 480 Probes, Roche), 2 µL of each forward and reverse primers (5 µmol/µL, Integrated DNA Technologies), 0.3 µL of Taqman Probe (10 µmol/L, Eurofins MWG Operon) and 0.7 µL of PCR-grade water (Qiagen). This study used same sequences of primers and probe as in Masago et al. [25]. The qPCR analysis started with 95°C for 15 min then followed by 45 amplification cycles at 95 °C for 10 s, 60 °C for 20 s and 72 °C for 10 s and finally cooling at 40°C for 30 s. To relate the crossing-point (C_p) values to the numbers of P22 DNA copies, a standard curve developed in our laboratory was used.

3. Results and Discussion

3.1. Hybrid membrane filtration-UV process: The concept and a brief rationale

UV disinfection is effective against a broad range of microorganisms and has unique advantages over other disinfection processes. As a unit operation, UV disinfection does not involve addition of chemicals and does not generate harmful disinfection by-products typical for chemical disinfection unit processes such as chlorination and ozonation.

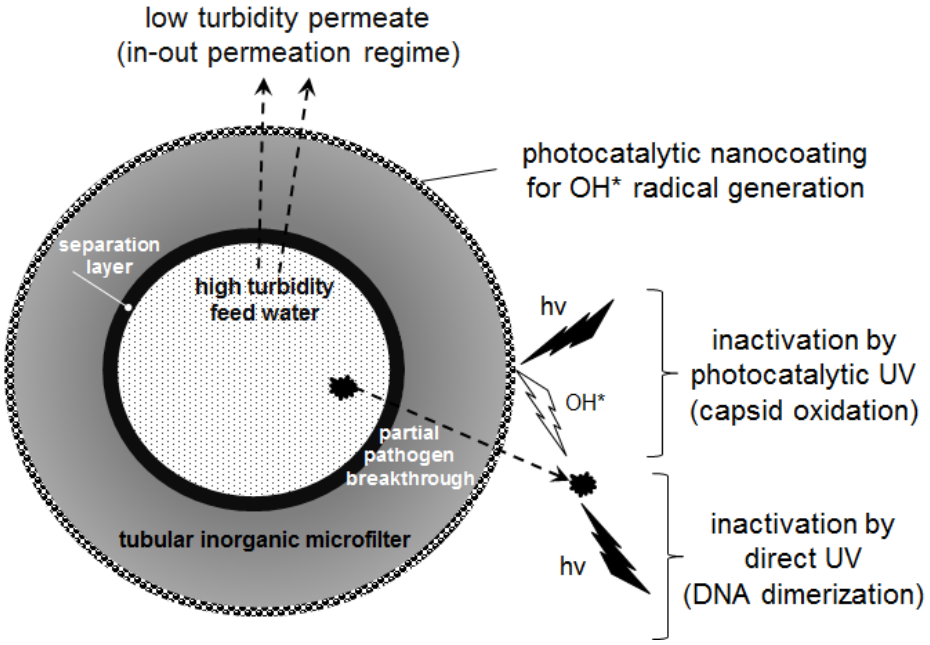

Figure 3: Conceptual illustration of the hybrid membrane filtration-UV disinfection process.

UV light is also effective for inactivating chlorine-resistant pathogens such as *Cryptosporidium* and *Giardia* protozoa (e.g. [35, 36]). A fundamental limitation of UV disinfection is that RNA-based microorganisms – a group that includes many EPA-regulated viruses such as enteroviruses, hepatitis A virus, and caliciviruses – are resistant to UV. Furthermore, some pathogens can repair UV-induced damage to their DNA. Another challenge is presented by water turbidity. Turbidity, when present at high

levels, limits UV light access to microorganisms and is known to diminish the efficacy of UV disinfection [37, 38].

The proposed novel approach combines microfiltration and UV disinfection into a hybrid photocatalytic process (Fig. 3) to overcome the above two challenges. The ultra- or microfiltration membrane operated in an inside-our geometry removes turbidity so that the UV irradiation is applied to a relatively turbidity-free permeate stream. The degree of turbidity removal is controlled by an appropriate choice of the membrane pore size.

Table 1: Rationale for the proposed UV-microfiltration hybrid process

Technology and its benefits		Challenges	How the challenge is addressed in a hybrid process
Photocatalytic UV disinfection	Photocatalytic UV is effective against a wide range of microbial pathogens.	Some pathogens are resistant to UV or can repair UV-induced damage	Catalytic oxidation at the membrane surface by ROS complements the physical effect of the direct UV.
	Chemicals demand and harm to receiving waters are minimal	Catalyst needs to be recovered	Membrane-supported catalyst is immobilized and does not need to be recovered.
	UV disinfection is catalytically enhanced	Efficiency is limited when turbidity is present	Turbidity is removed by the microfilter “upstream” from the UV reactor
Membrane filtration	Membranes provide absolute barrier to pathogens	Lower pore size for removal of smaller pathogens results in lower permeate fluxes	Redundancy introduced with catalytic UV disinfection enables trade-offs in pore sizes and product water fluxes

At the same time, the membrane serves as a support for photocatalytic nanoparticles immobilized on the outer (i.e. permeate) membrane surface exposed to the UV light. The catalytic enhancement of UV disinfection is due to non-specific chemical oxidation by reactive oxygen species (ROS) catalytically generated at the membrane surface. The oxidation complements direct UV to pose a “dual threat” to pathogens with direct UV targeting microorganism’s DNA and ROS damaging cellular membrane (in cases of

bacteria and protozoa) or viral capsid (in case of viruses). These and several other advantages of the proposed hybrid process are summarized in Table 1.

3.2. Efficacy of disinfection by direct UV irradiation

First, batch experiments were conducted to determine UV fluence as a function of UV exposure time by using KI/KIO_3 solution as an indicator. Following the procedure described in section 2.7 (see eq. (1)), values of UV fluence were calculated (see SC, Fig. S1). The exposure time was considered to be equal to the retention time of permeate solution in the quartz sleeve. The results show that fluence increased linearly with exposure time (see SI). Second, the log removal (LRV) of viable P22 was measured as a function of UV fluence LRV is defined as

$$LRV(t) = -log\left(\frac{N}{N_0}\right) \quad (2)$$

where N_0 and N are P22 concentrations in the batch reactor at time 0 and time t into the reaction, respectively. The kinetics of P22 inactivation by UV light could be approximated (Fig. 4) by the Collins-Selleck model [39, 40]:

$$ln\left(\frac{N}{N_0}\right) = -\Lambda_{CS}[ln(\Phi) - \ln(b)] \quad (3)$$

where Λ_{CS} is Collins-Selleck coefficient of specific lethality and b is the lag coefficient. Based on the fit of experimental data to eq. (3), the following values of these two coefficients were determined: Λ_{CS} = 1.972; b = 0.376 mW·s/cm^2. With $\Phi(t)$ and $LRV(\Phi)$ dependencies determined, the dependence of the efficacy of disinfection (expressed in terms of LRV) by direct UV irradiation on the UV exposure time was established.

The small negative “lag” described by b (i.e. non-zero extrapolated value of P22 inactivation based on the fit given by eq. (3)) is attributed to an experimental error.

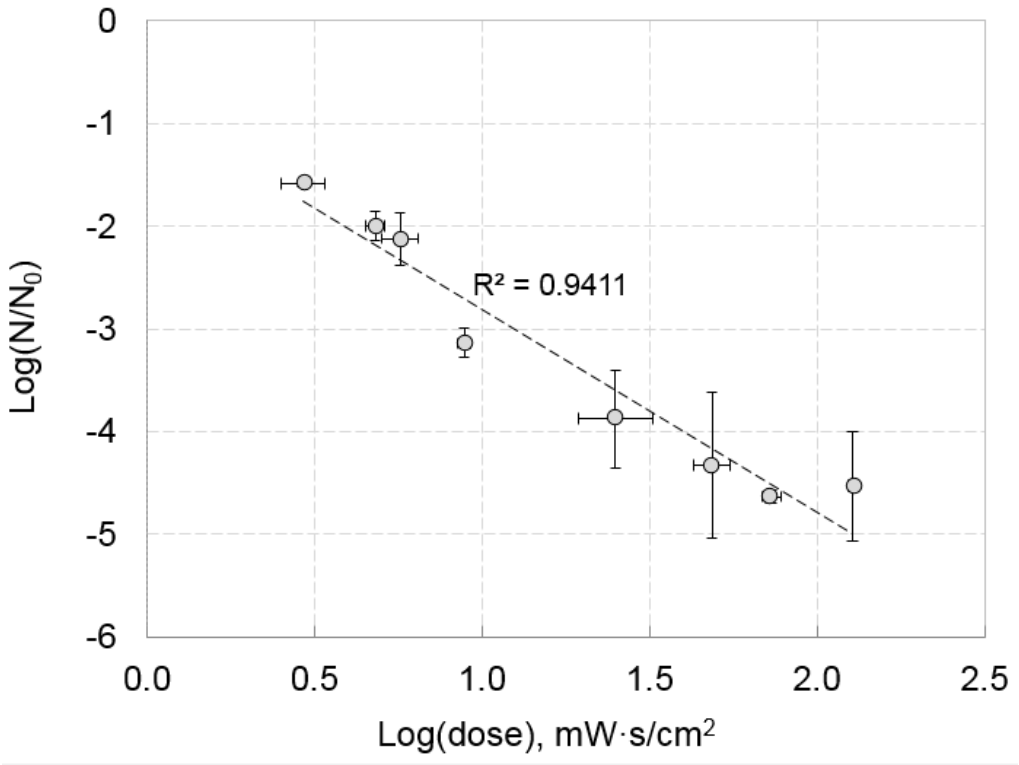

Figure 4. Log removal of viable P22 bacteriophage as a function of UV fluence. Error bars represent standard deviations (n=3).

The decelerating kinetics described by the Collins-Selleck model could be a consequence of P22's being shielded from the UV light by residual components of the virus growth media.

3.3. Characterization of the tubular ceramic membrane

SEM images of the as-received tubular ceramic membrane and the same membrane coated with TiO_2 P25 nanocatalyst are presented in Fig. 5. The separation layer of this 0.8 µm nominal pore size membrane is on the inner wall of the membrane channel making the membrane suitable for use in the inside-out flow geometry only.

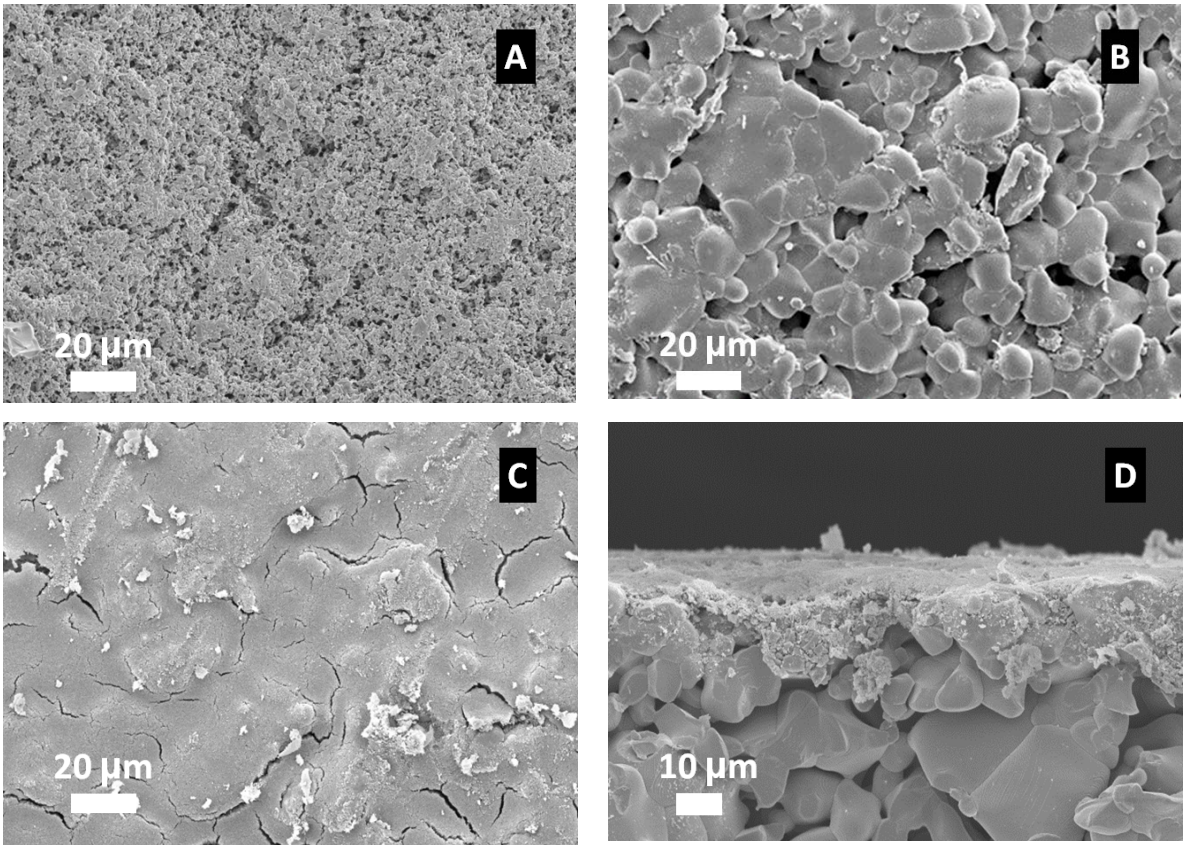

Figure 5. Scanning electron micrographs of the tubular ceramic membrane: A) planar view of the inner surface, B) planar view of the uncoated outer surface, C) planar view of the TiO_2-coated outer surface, and D) the cross-sectional view of the coated outer surface of the tubular ceramic membrane.

Accordingly, the inner (feed) surface of the membrane has a finer pore structure (Fig. 5A) than the more porous and rough outer (permeate) surface composed of larger TiO_2 grains (Fig. 5B). The coating-induced morphological changes of the outer membrane surface could be clearly observed: the 10-layer coating covered the outer surface of the membrane with a layer of TiO_2 P25 that is relatively smooth but cracked (Fig. 5C). The cracking might be due to the high roughness of the underlying membrane surface, which could lead to an uneven tensile stress in the coating [41, 42]. The coating was not homogeneous over the entire membrane surface with some portions of the membrane coated with a denser catalyst layer. The reasons were not clear and an additional study would be required to optimize the coating process.

Coating the permeate surface with a TiO_2 layer led to ~ 40% decline in the permeability of the membrane. Figure 6A illustrates how the specific permeate flux, J , of uncoated and coated membranes changed with the time of filtration of ultrapure water first in the absence of UV and then after exposed to UV irradiation. In the absence of UV (i.e. during the first 60 min of the filtration test) the specific permeate flux through an uncoated membrane declined by ~ 17.5%. A declining trend for pure water permeate flux for ceramic membranes has been reported in the past [43-45] and attributed by Mendret et al [45] to the very slow hydration of the membrane surface. However, given the very large nominal pore size (0.8 μm) of the membrane employed in our study, hydration shell should be much thinner than the pore size so that hydration can be eliminated as the reason for flux decline. A part of the reason for this flux behavior is the change in water temperature (Fig. 6B) as it decreased throughout the first 60 min of the test from its initial value (23 ^{0}C) towards the lower temperature of the ambient air (20.3 ^{0}C). When the temperature induced changes were factored out by normalizing values of the specific permeate flux by viscosity, the resulting time dependence of membrane permeability still showed a 16.5% decline (Fig. 6C). Tentatively, we attribute the observed flux behavior to the re-arrangement of loosely affixed TiO_2 particles due to permeate flow.

A)

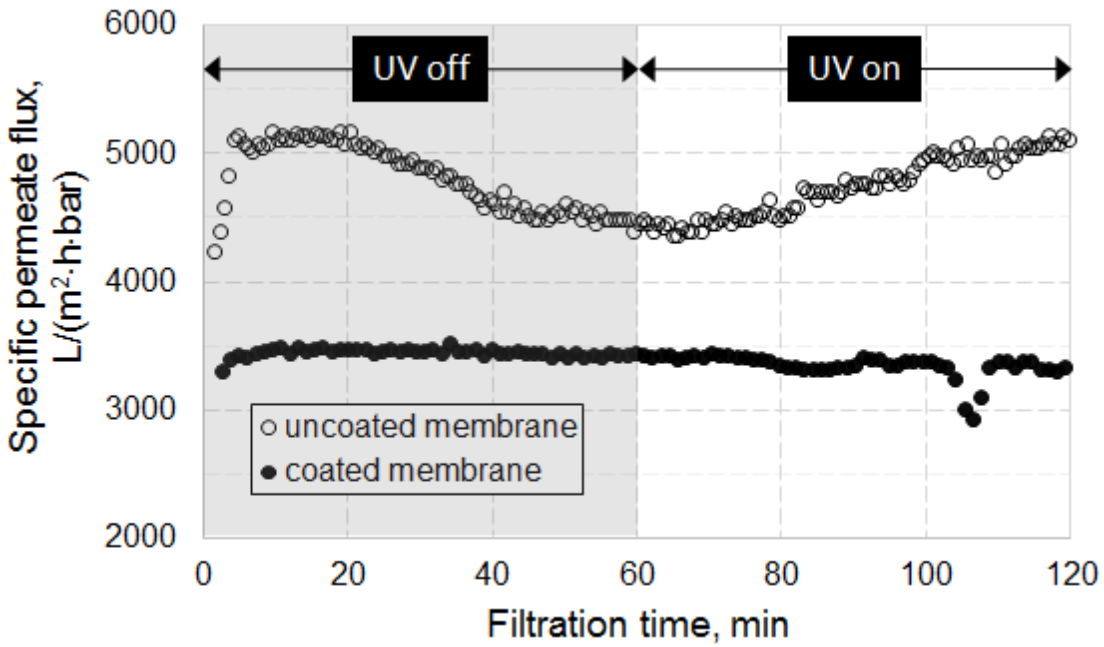

B)

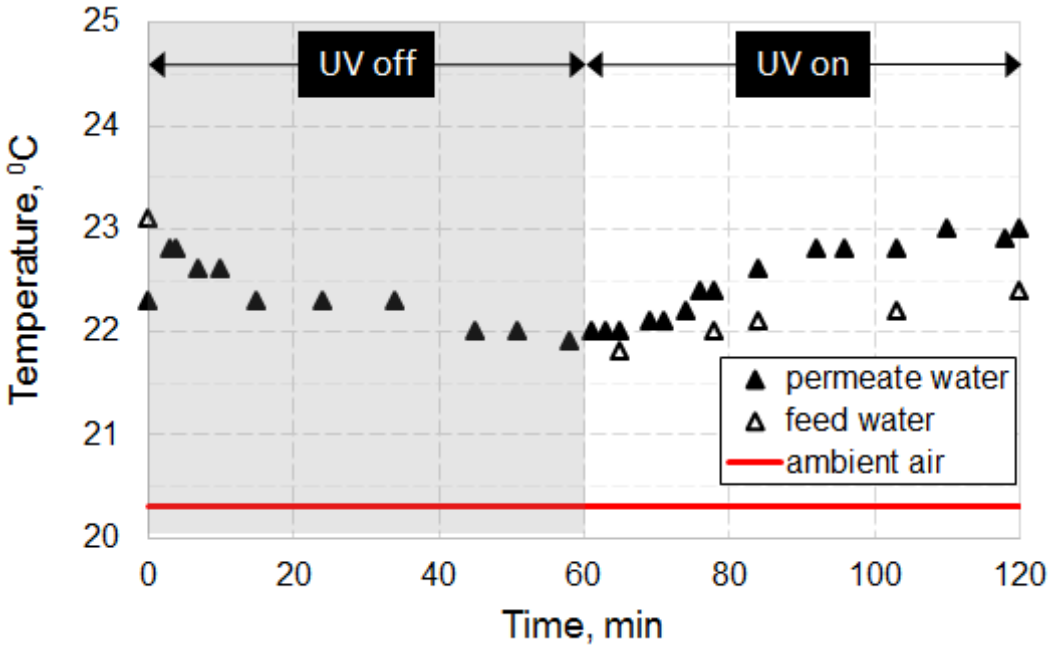

C)

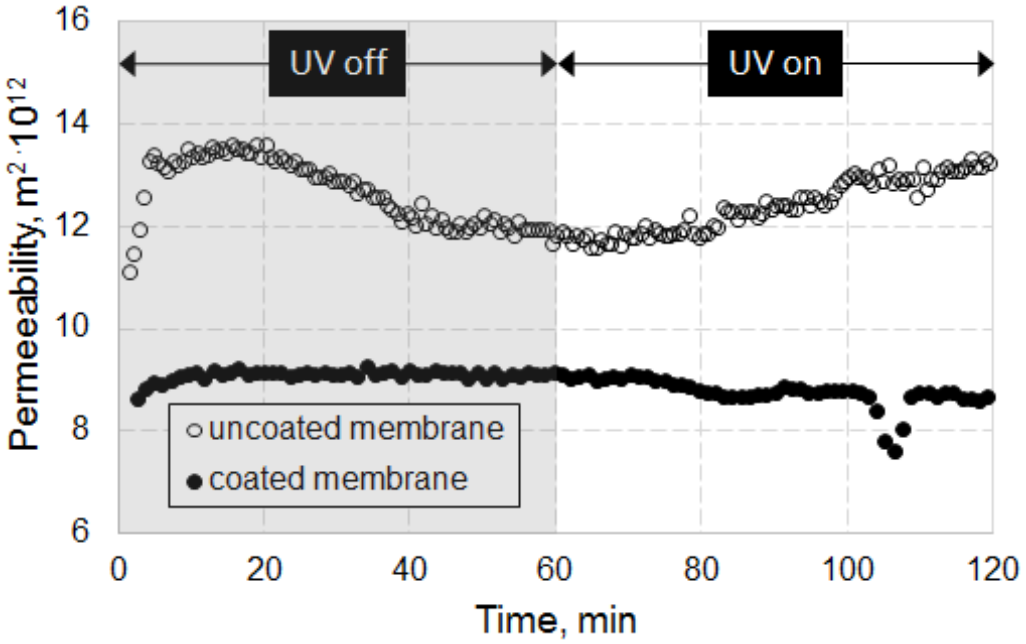

Figure 6. Specific permeate flux of ultrapure water (A), temperature of ambient air, feed water and permeate water (B), and permeability (C) as functions of filtration time for uncoated and TiO_2 P25-coated membranes.

When the outer membrane surface was illuminated by the UV light the permeate flux (Fig. 6A) started to increase. We attribute this increase to higher temperature (Fig. 6B) and resulting lower viscosity of the permeating water due to membrane heating by the UV light. The temperature effect could not fully explain away the increase in flux - the permeability still increased with time (Figure 6C) in the presence of UV. We attribute this fact to errors in temperature measurements: collecting a sample for temperature measurements takes time during which the water in the sample can cool down.

Mendret et al [45] reported similar UV-induced increases in permeate flux and explained them as stemming from photoinduced hydrophilicity [46, 47]. In our case though it was the porous permeate side of the membrane, and not the permeability-controlling separation layer, that was exposed to UV irradiation (Fig. 3). Because the membrane is not transparent to UV, only a thin sublayer of the membrane on its permeate side could have experienced photoinduced changes in surface hydrophilicity. The resulting

improved wettability of this part of porous structure could not have been responsible for the observed increase in the overall permeability of the membrane.

Notably, the permeate flux of the coated membrane did not show a similar dependence on filtration time in the absence of UV light nor did it show a response to the UV irradiation. This behavior can be rationalized by posing that a) loose particles in the membrane are stabilized during the coating and sintering procedures, and b) energy of the UV irradiation is absorbed by the coating and not dissipated as heat that can increase the temperature of the permeating solution.

4. Removal and inactivation of bacteriophage P22

Separate experiments were performed on the removal and inactivation of P22 bacteriophage in three treatment processes: 1) MF only, 2) hybrid UV-MF process with an uncoated membrane, and 3) hybrid UV-MF process with a TiO_2-coated membrane. The dependence of permeate flux on filtration time in these tests is shown in Fig. S2 (see SC file). Figure 7 summarizes LRV data for viable P22 by the four processes for six different times into the filtration process (also see SC, Table S3):

1) Among all processes tested, microfiltration, applied alone, was the least effective in removing viable P22 (LRV = 0.5 ± 0.5). The low removal rate was due to the large nominal pore size of the microfilter (0.8 µm) relative to the hydrodynamic diameter of P22 bacteriophage (d_p = 68.8 nm) [48]. The overall removal of viable P22 by the membrane can be attributed to a combination of adsorption, size exclusion, and inactivation upon contact with the membrane surface. Despite the mismatch between the pore size and virus diameter, size exclusion may still be possible because the membrane pore size distribution is of finite width and may include very small pores.

2) The estimated (see section 2.8) inactivation by direct UV was very stable throughout the entire 60 min of filtration with an average LRV of 1.6 ± 0.1. The contribution of the UV process to bacteriophage inactivation is due to UV's germicidal

effect, which reduces the number of infective viruses but not the total number of viral particles.

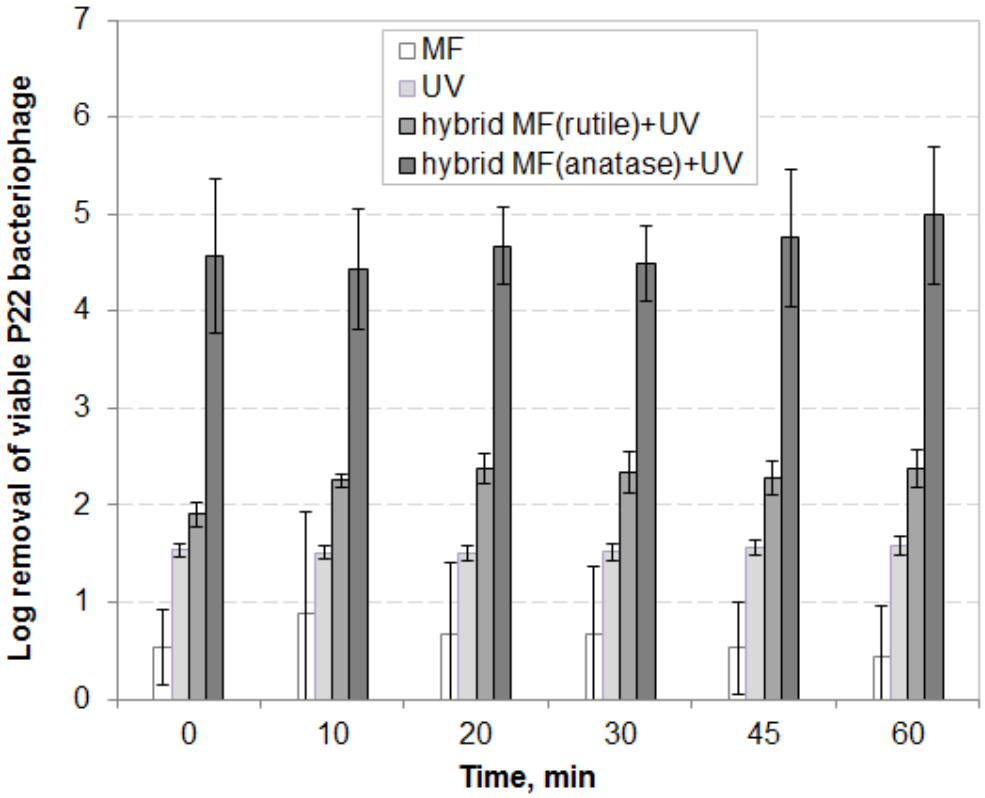

Figure 7. Inactivation and/or removal of viable P22 bacteriophage by 1) microfiltration only, 2) direct UV only, 3) non-photocatalytic hybrid UV-MF process, and 4) photocatalytic hybrid UV-MF process. Error bars represent standard deviations (n=3).

3) Averaged over filtration time, the LRV removal of viable P22 by the hybrid UV-MF process with an uncoated MF membrane (2.3 ± 0.2) was not statistically different from the arithmetic sum of LRVs achieved by the two constituent processes, UV and MF with uncoated membrane - applied separately.

4) By contrast, the hybrid UV-MF process with a membrane coated with TiO_2 photocatalyst resulted in an average LRV of 5.0 ± 0.7, which was more than two times higher than the corresponding value for the hybrid UV-MF test with uncoated membranes.

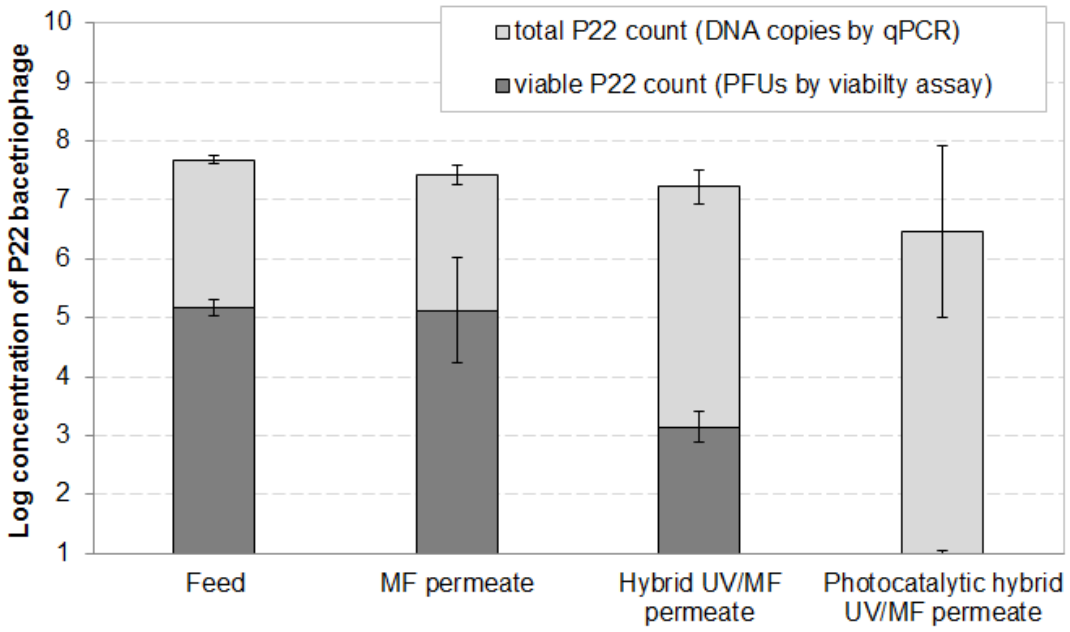

Figure 8: Log concentration of viable and total bacteriophage P22 in the feed solution and in the permeate 30 min into the filtration process. Error bars correspond to standard deviations.

The synergistic effect was due to the membrane-based photocatalysis, wherein reactive oxygen species (ROS) generated at the surface of TiO_2 nanoparticles of the coating provide non-specific oxidation that complemented the effect of direct UV. While direct UV inactivates viruses by dimerizing their DNA [49], ROS contribute to disinfection by oxidizing the protein capsid of viruses. As mentioned earlier, this contribution of photocatalysis to the overall removal of viable viruses is especially important because, in contrast to direct UV, it can inactivate RNA viruses.

Figure 8 provides absolute values of the total concentration of P22 and the concentration of viable P22 in the effluent after 30 min of operation of each of the three treatment processes. The total virus count (i.e. viable and non-infective fractions together) in feed and permeate samples was estimated based on DNA copy counts measured by qPCR. The data show that the photocatalytic UV-MF process is effective in inactivating viable P22 even though the reduction of the total virus is not significant. The large value of the LRV recorded for the hybrid process points to the possibility of employing membranes with even larger pore size to enable higher flow rates.

3.6 Potential applications in water treatment

The proposed hybrid process can mitigate two salient disadvantages of UV disinfection: resistance of certain environmentally important pathogens to UV disinfection and low efficacy of UV light when applied to highly turbid waters. Coupling microfiltration with photocatalytic UV process can make disinfection of highly turbid or large flow rate streams (e.g. ballast and storm water) more efficient in terms of the required UV dose for a given level of disinfection. This improvement, however, would likely come at the expense of membrane fouling and, therefore, a higher cost of membrane operation.

A possible application for the proposed hybrid process and an important environmentally-relevant example of a high flow rate operation requiring disinfection is ballast water treatment. Recent International Marine Organization D2 regulations impose limits on the concentration of microbes in ballast water. According to these regulations, all vessels built after January 1, 2016 must comply with the U.S. Coast Guard Discharge Standards Phase 2 that require that no more than 10^3 bacteria and 10^4 viruses are present in 100 mL of treated ballast water. Given the very small size of microorganisms and the large flow rates typical for ballast water treatment, complete physical removal of bacteria and especially viruses is unlikely, which makes disinfection a critical second barrier. It is now recognized that no single process efficiently removes the wide range of potential invasive species in ballast water and that a combination of technologies must be considered [50]. A combination of filtration and subsequent disinfection has been identified as the best available treatment [51]. To date, UV disinfection has been applied as a stand-alone unit [52-56] and in combination with physical separation methods that use filters [57, 58] and hydrocyclones [59, 60]. The prior history of adoption of these technologies by the shipping industry bodes well for the application of new hybrid technologies that combine filtration and UV light

Innovative reflector designs can further facilitate field applications of the proposed photocatalytic membrane reactor. For example, we envision a reflector with a parabolic

profile of corrugation as a large surface area lens that focuses incident light on tubular filters positioned in foci of the parabolas. Finally, membranes can support a broad range of photocatalytic materials including high efficiency UV and visible-light photocatalysts that tap into solar energy and may enable low cost disinfection.

4. Conclusions

We report on the first application of photocatalytic membranes for virus removal and inactivation. In the proposed hybrid technology, UV light is focused on a TiO_2-coated outer surface of a tubular ceramic membrane operated in an inside-out geometry. The hybrid process is evaluated with respect to removal and inactivation of P22 bacteriophage, a model virus. The kinetics of P22 inactivation by direct UV was first evaluated in a separate set of tests in a batch UV reactor and found to fit Collins-Selleck model. To gauge the performance of the hybrid UV-microfiltration process, a number of crossflow filtration tests were performed with and without UV light as well as with and without photocatalytic coating on the membrane. Compared to stand-alone microfiltration, stand-alone UV disinfection and UV-microfiltration with a non-photocatalytic membrane, the hybrid photocatalytic UV-microfiltration process was considerably more effective in inactivating the virus. Average values of log removal of viable P22 by these four processes were 0.5 ± 0.5, 1.6 ± 0.1, 2.3 ± 0.2, and 5.0 ± 0.7, respectively. The proposed hybrid process can mitigate two salient disadvantages of disinfection by direct UV: resistance of certain environmentally important pathogens to UV and low efficacy of UV disinfection when applied to highly turbid waters. Virus removal and inactivation can be regulated by the choice of the membrane pore size, design of the photocatalytic coating, and by controlling UV fluence applied to the permeate stream. Potential applications of the hybrid UV-microfiltration technology include treatment of turbid, high fouling potential and high flow rate streams that cannot be cost-effectively disinfected by other means.

Acknowledgements

This research has been supported in part by the U.S. National Science Foundation (award no. IIA 1243433) and in part by Michigan State University Foundation (award no 71-1624). The assistance of Mr. Craig Burk (Department of Civil and Environmental Engineering, MSU) with designing the dip-coating apparatus is gratefully acknowledged. We would also like to thank Dr. Eldon Case (MSU Department of Chemical Engineering and Materials Science) for providing access to the furnace for membrane sintering as well as Evonik Industries for providing free samples of Aeroxide TiO_2 P25 powder.

List of Figures

References

[1] A. Zakersalehi, H. Choi, J. Andersen, D.D. Dionysiou, Photocatalytic ceramic membranes, in: E.M.V. Hoek, V.V. Tarabara (Eds.) Encyclopedia of Membrane Science and Technology, John Wiley & Sons, 2013.

[2] S. Leong, A. Razmjou, K. Wang, K. Hapgood, X. Zhang, H. Wang, TiO2 based photocatalytic membranes: A review, J. Membr. Sci., 472 (2014) 167-184.

[3] T. Matsunaga, R. Tomoda, T. Nakajima, H. Wake, Photoelectrochemical sterilization of microbial cells by semiconductor powders, FEMS Microbiol. Lett., 29 (1985) 211-214.

[4] M.N. Chong, B. Jin, C.W.K. Chow, C. Saint, Recent developments in photocatalytic water treatment technology: A review, Water Res., 44 (2010) 2997-3027.

[5] O.K. Dalrymple, E. Stefanakos, M.A. Trotz, D.Y. Goswami, A review of the mechanisms and modeling of photocatalytic disinfection, Appl. Catal. B, 98 (2010) 27-38.

[6] S. Pigeot-Remy, F. Simonet, E. Errazuriz-Cerda, J.C. Lazzaroni, D. Atlan, C. Guillard, Photocatalysis and disinfection of water: Identification of potential bacterial targets, Appl. Catal. Environ., 104 (2011) 390-398.

[7] J.C. Sjorgen, R.A. Sierka, Inactivation of phage MS2 by iron-aided titanium dioxide photocatalysis, Appl. Environ. Microbiol. , 60 (1994) 344-347.

[8] Q. Li, M.A. Page, B.J. Marinas, J.K. Shang, Treatment of coliphage MS2 with palladium-modified nitrogen-doped titanium oxide photocatalyst illuminated by visible light, Environ. Sci. Technol., 42 (2008) 6148-6153.

[9] J. Lee, K. Zoh, G. Ko, Inactivation and UV disinfection of murine norovirus with TiO2 under various environmental conditions, Appl. Environ. Microbiol., 74 (2008) 2111-2117.

[10] D. Gerrity, H. Ryu, J. Crittenden, M. Abbaszadegan, Photocatalytic inactivation of viruses using titanium dioxide nanoparticles and low-pressure UV light, J. Environ. Sci. Health A, 43 (2008) 1261-1270.

[11] H. Choi, M.G. Antoniou, A.A. de la Cruz, E. Stathatos, D.D. Dionysiou, Photocatalytic TiO2 films and membranes for the development of efficient wastewater treatment and reuse systems, Desalination, 202 (2007) 199-206.

[12] H. Zhang, H. Zhao, P. Liu, S. Zhang, G. Li, Direct growth of hierarchically structured titanate nanotube filtration membrane for removal of waterborne pathogens, J. Membr. Sci., 343 (2009) 212-218.

[13] N. Ma, X. Fan, X. Quan, Y. Zhang, Ag–TiO2/HAP/Al2O3 bioceramic composite membrane: Fabrication, characterization and bactericidal activity, J. Membr. Sci., 336 (2009) 109-117.

[14] L. Liu, Z.Y. Liu, H.W. Bai, D.D. Sun, Concurrent filtration and solar photocatalytic disinfection/degradation using high-performance Ag/TiO2 nanofiber membrane, Water Res., 46 (2012) 1101-1112.

[15] R. Goei, T.-T. Lim, Ag-decorated TiO2 photocatalytic membrane with hierarchical architecture: Photocatalytic and antibacterial activities, Water Res., 59 (2014) 207-218.

[16] R.A. Damodar, S.-J. You, H.-H. Chou, Study the self cleaning, antibacterial and photocatalytic properties of TiO2 entrapped PVDF membranes, J. Hazard. Mater., 172 (2009) 1321-1328.

[17] M. Pelaez, N.T. Nolan, S.C. Pillai, M.K. Seery, P. Falaras, A.G. Kontos, P.S.M. Dunlop, J.W.J. Hamilton, J.A. Byrne, K. O'Shea, M.H. Entezari, D.D. Dionysiou, A review on the visible light active titanium dioxide photocatalysts for environmental applications, Appl. Catal. Environ., 125 (2012) 331-349.

[18] A. Julbe, D. Farrusseng, C. Guizard, Porous ceramic membranes for catalytic reactors— overview and new ideas, J. Membr. Sci., 181 (2001) 3-20.

[19] K. Nakata, A. Fujishima, TiO2 photocatalysis: Design and applications, J. Photochem. Photobiol. C, 13 (2012) 169- 189.

[20] F. Bosc, A. Ayral, C. Guizard, Mesoporous anatase coatings for coupling membrane separation and photocatalyzed reactions, J. Membr. Sci., 265 (2005) 13-19.

[21] C.M. Teschke, K.N. Parent, 'Let the phage do the work': Using the phage P22 coat protein structures as a framework to understand its folding and assembly mutants, Virology, 401 (2010) 119-130.

[22] K.N. Parent, R. Khayat, L.H. Tu, M.M. Suhanovsky, J.R. Cortines, C.M. Teschke, J.E. Johnson, T.S. Baker, P22 Coat Protein Structures Reveal a Novel Mechanism for Capsid Maturation: Stability without Auxiliary Proteins or Chemical Crosslinks, Structure, 18 (2010) 390-401.

[23] K.N. Parent, R.S. Sinkovits, M.M. Suhanovsky, C.M. Teschke, E.H. Egelman, T.S. Baker, Cryo-reconstructions of P22 polyheads suggest that phage assembly is nucleated by trimeric interactions among coat proteins, Physical Biology, 7 (2010).

[24] J.R. Cortines, P.R. Weigele, E.B. Gilcrease, S.R. Casjens, C.M. Teschke, Decoding bacteriophage P22 assembly: Identification of two charged residues in scaffolding protein responsible for coat protein interaction, Virology, 421 (2011) 1-11.

[25] Y. Masago, T. Shibata, J.B. Rose, Bacteriophage P22 and Staphylococcus aureus attenuation on nonporous fomites as determined by plate assay and quantitative PCR, Appl. Environ. Microbiol., 74 (2008) 5838-5840.

[26] C.P. Shen, M.S. Phanikumar, T.T. Fong, I. Aslam, S.P. McElmurry, S.L. Molloy, J.B. Rose, Evaluating bacteriophage P22 as a tracer in a complex surface water system: The Grand River, Michigan, Environ. Sci. Technol., 42 (2008) 2426-2431.

[27] B. Ohtani, O.O. Prieto-Mahaney, D. Li, R. Abe, What is Degussa (Evonik) P25? Crystalline composition analysis, reconstruction from isolated pure particles and photocatalytic activity test, J. Photochem. Photobiol. A, 216 (2010) 179-182.

[28] W.Y. Wang, A. Irawan, Y. Ku, Photocatalytic degradation of Acid Red 4 using a titanium dioxide membrane supported on a porous ceramic tube, Water Res., 42 (2008) 4725-4732.

[29] R.O. Rahn, P. Xu, S.L. Miller, Dosimetry of room-air germicidal (254 nm) radiation using spherical actinometry, Photochem. Photobiol., 70 (1999) 314.

[30] R.O. Rahn, J. Bolton, M.I. Stefan, The iodide/iodate actinometer in UV disinfection: Determination of the fluence rate distribution in UV reactors, Photochem. Photobiol., 82 (2006) 611-615.

[31] R.O. Rahn, S. Echols, Iodide/iodate chemical actinometry using spherical vessels for radiation exposure as well as for monitoring absorbance changes, Photochem. Photobiol., 86 (2010) 990-993.

[32] R.O. Rahn, Potassium iodide as a chemical actinometer for 254 nm radiation: Use of iodate as an electron scavenger, Photochem. Photobiol., 66 (1997) 450-455.

[33] R.O. Rahn, M.I. Stefan, J.R. Bolton, E. Goren, P.S. Shaw, K.R. Lykke, Quantum yield of the iodide-iodate chemical actinometer: Dependence on wavelength and concentration, Photochem. Photobiol., 78 (2003) 146-152.

[34] EPA, Method 1602: Detection of male-specific (F+) and somatic coliphage in water by single agar layer (SAL) procedure, in: Office of Water, Engineering and Analysis Division, Washington, DC, 2001.

[35] Z. Bukhary, J. Hargy, B. Bolton, B. Dussert, J. Clancy, Inactivation of Cryptosporidium parvum oocysts using medium=pressure ultraviolet light, in: Proceedings of AWWA annual conference, Dallas, TX, 1998.

[36] K.G. Linden, G.-A. Shin, G. Faubert, W. Cairns, M.D. Sobsey, UV disinfection of Giardia lamblia cysts in water, Environ. Sci. Technol., 36 (2002) 2519-2522.

[37] F. Loge, K. Bourgeous, R. Emerick, J. Darby, Variations in wastewater quality parameters influencing UV disinfection performance: Relative impact of filtration, J. Environ. Eng. ASCE, 127 (2001) 832-837.

[38] J. Oppenheimer, T. Gillogly, G. Stolarik, R. Ward, Comparing the efficiency of low and medium pressure UV light for inactivating Giardia muris and Cryptosporidium parvum in waters with low and high levels of turbidity, in: Annual Conference and Exhibition of the American Water Works Association, New Orleans, LA, 2002.

[39] H. Collins, R. Selleck, G.C. White, Problems in obtaining adequate sewge dinsinfection, J. San. Eng. Div. ASCE, 97 (1971) 549-562.

[40] R. Selleck, B. Saunier, Kinetics of bacterial deactivation with chlorine, J. Environ. Eng. ASCE, 104 (1978) 1197-1212.

[41] C.J. Brinker, T.L. Ward, R. Sehgal, N.K. Raman, S.L. Hietala, D.M. Smith, D.W. Hua, T.J. Headley, Ultramicroporous silica-based supported membranes, J. Membr. Sci., 77 (1993) 165-179.

[42] J.H. Park, W.S. Kim, D.-H. Jo, J.S. Kim, J.M. Park, Effect of Ce conversion underlayer coating on the photo-catalytic activity of TiO2 sol-gel film deposited on hot-dip GI, J. Ind. Eng. Chem., 20 (2014) 1965-1972.

[43] H. Zhang, X. Quang, S. Chen, H. Zhao, Y. Zhao, Fabrication ofphotocatalytic membrane and evaluation its efficiencyinremoval oforganic pollutants from water, Separ. Purif. Technol., 50 (2006) 147-155.

[44] E. Chevereaua, N. Zouaouib, L. Limousya, P. Dutourniéa, S. Déonc, P. Bourseaud, Surface properties of ceramic ultrafiltration TiO2 membranes: Effects of surface equilibriums on salt retention, Desalination, 255 (2010) 1-8.

[45] J. Mendret, M. Hatat-Fraile, M. Rivallin, S. Brosillon, Hydrophilic composite membranes for simultaneous separation and photocatalytic degradation of organic pollutants, Separ. Purif. Technol., 111 (2013) 9-19.

[46] R. Wang, K. Hashimoto, A. Fujishima, M. Chikuni, E. Kojima, A. Kitamura, M. Shimohigoshi, T. Watanabe, Light-induced amphiphilic surfaces, Nature, 388 (1997) 431-432.

[47] R. Wang, K. Hashimoto, A. Fujishima, M. Chikuni, E. Kojima, A. Kitamura, M. Shimohigoshi, T. Watanabe, Photogeneration of highly amphiphilic TiO2 surfaces, Adv. Mater., 10 (1998) 135-138.

[48] E.V. Pasco, H. Shi, I. Xagoraraki, S.A. Hashsham, K.N. Parent, M.L. Bruening, V.V. Tarabara, Polyelectrolyte multilayers as anti-adhesive membrane coatings for virus concentration and recovery, J. Membr. Sci., 469 (2014) 140-150.

[49] W. Kowalski, UVGI for air and surface disinfection, in: Ultraviolet Germicidal Irradiation Handbook, 2009.

[50] E. Tsolaki, E. Diamadopoulos, Technologies for ballast water treatment: A review, J. Chem. Technol. Biotechnol., 85 (2010) 19-32.

[51] A.N. Perakis, Z. Yang, Options for nonindigenous species control and their economic impact on the Great Lakes and St. Lawrence seaway: A survey. , Mar. Technol., 40 (2003) 34-41.

[52] S. Montani, L. Mksumpun, K. Ichimi, Chemical and physical treatments for destruction of phytoflagellate cysts, J. Mar. Biotechnol., 2 (1995) 179-181.

[53] A.A. Cangelosi, I.T. Knight, M. Balcer, D. Wright, R. Dawson, C. Blatchley, The Great Lakes Ballast Technology Demonstration project: Biological effectiveness test program (including MV Regal Princess trials), in: International Maritinme Organization 1st International Ballast Water Treatment R&D Symposium, London, UK, 2001, pp. 88-94.

[54] M.A. Champ, Marine Testing Board for certification of ballast water technologies, Mar. Poll. Bull., 44 (2002) 1327-1335.

[55] J. Sassi, S. Viitasalo, J. Rytkönen, E. Leppäkoski, Experiments with ultraviolet light, ultrasound and ozone technologies for onboard ballast water treatment (VTT Research Notes 2313), in, VTT Technical Research Centre of Finland, 2005, pp. 1-80.

[56] X.P. Kong, Y.M. Zhu, M.X. Zhang, X.J. Sun, W. Zhang, Simulated experiment on minimizing the presence of chlorella and bacteria in ballast water by combination of micro-hole filtration and UV radiation, J. Adv. Oxid. Technol., 10 (2007) 186-188.

[57] B. Nilsen, H. Nilsen, T. Mackey, The Optimar ballast system, in: International Maritinme Organization 1st International Ballast Water Treatment R&D Symposium, London, UK, 2001, pp. 126-136.

[58] D.A. Wright, R. Dawson, C.E. Orano-Dawson, S.M. Moesel, A test of the efficacy of a ballast water treatment system aboard the vessel Coral Princess, Mar. Technol., 44 (2007) 57-67.

[59] T.F. Sutherland, C.D. Levings, C.C. Elliott, W.W. Hesse, Effect of a ballast water treatment system on survivorship of natural populations of marine plankton, Mar. Ecol. Prog. Ser., 210 (2001) 139-148.

[60] T.F. Sutherland, C.D. Levings, S. Petersen, W.W. Hesse, Mortality of zooplankton and invertebrate larvae exposed to cyclonic pre-treatment and ultraviolet radiation, Mar. Technol. Soc. J., 37 (2003) 3-12.